Monthly Notices of the ROYAL ASTRONOMICAL SOCIETY

MNRAS **516,** 3092–3101 (2022) https://doi.org/10.1093/mnras/stac2439
Advance Access publication 2022 September 2

SDSS IV MaNGA - star-formation driven biconical outflows in face-on galaxies

D. Bizyaev [1,2★] Yan-Mei Chen,[3,4] Yong Shi [3,4] Namrata Roy [5] Rogerio Riffel [6,8] Rogemar A. Riffel [7,8] and José G. Fernández-Trincado[9]

[1]*Apache Point Observatory and New Mexico State University, Sunspot, NM 88349, USA*
[2]*Sternberg Astronomical Institute, Moscow State University, Moscow, 119234, Russia*
[3]*School of Astronomy and Space Science, Nanjing University, Nanjing 210093, China*
[4]*Key Laboratory of Modern Astronomy and Astrophysics (Nanjing University), Ministry of Education, Nanjing 210093, China*
[5]*Department of Astronomy and Astrophysics, University of California, 1156 High Street, Santa Cruz, CA 95064, USA*
[6]*Departamento de Astronomia, Instituto de Física, Universidade Federal do Rio Grande do Sul, CP 15051, 91501-970, Porto Alegre, RS, Brazil*
[7]*Departamento de Física, Centro de Ciências Naturais e Exatas, Universidade Federal de Santa Maria, 97105-900, Santa Maria, RS, Brazil*
[8]*Laboratório Interinstitucional de e-Astronomia - LIneA, Rua Gal. José Cristino 77, Rio de Janeiro, RJ - 20921-400, Brazil*
[9]*Instituto de Astronomía, Universidad Católica del Norte, Av. Angamos 0610, Antofagasta, Chile*

Accepted 2022 August 26. Received 2022 August 25; in original form 2022 June 11

ABSTRACT

We find 132 face-on and low inclination galaxies with central star formation driven biconical gas outflows (FSFB) in the SDSS MaNGA (Mapping Nearby Galaxies at APO) survey. The FSFB galaxies show either double peaked or broadened emission line profiles at their centres. The peak and maximum outflow velocities are 58 and 212 km s^{-1}, respectively. The gas velocity dispersion reveals a mild dependence on the central star formation surface density compatible with models of gas dispersion powered by the Jeans instability in gas clumps or by gas turbulence dissipation. We estimate the gas outflow rate and conclude that the central gas depletion time does not depend on galactic mass. In turn, the ratio of the gas outflow rate to the gas consumption rate by the star formation is low in massive galaxies and high in low mass objects, while the star formation is a more rapid process of the gas consumption. We compare properties of the FSFB galaxies with a control sample of 375 comparison galaxies and find that the FSFB objects have high central concentration of star formation and also younger central stellar population with respect to their periphery. We analysed the environment of the galaxies and identified nearby satellites and elements of low surface brightness structure. We see that many tidal-enhanced features that can be assigned to early and intermediate stages of galactic interaction are much more frequent in the FSFB galaxies with respect to the comparison sample. We conclude that the gas should be replenished via the accretion from small satellites.

Key words: ISM: jets and outflows – galaxies: interactions – galaxies: ISM – galaxies: kinematics and dynamics – galaxies: star formation – galaxies: structure.

1 INTRODUCTION

Gas outflows from central regions of galaxies can be powered not only by active galactic nuclei (AGN) but also by star formation bursts (Lehnert & Heckman 1995, 1996; Strickland & Heckman 2007; Heckman et al. 2015). Multiphase gas outflows driven by star formation bursts in galaxies without AGNs are common in both nearby (Veilleux, Cecil & Bland-Hawthorn 2005; Chen et al. 2010) and distant (Rubin et al. 2014; Davies et al. 2018) galaxies. While in most galaxies the outflows eject gas in all directions (Lehnert & Heckman 1996), some objects, including nearby starburst galaxies M 82 and NGC 253, show biconical star formation driven superwinds that start from galactic centres (Heckman, Armus & Miley 1990; Lehnert, Heckman & Weaver 1999). Numerical simulations predict that central biconical outflows are common in galaxies (Tenorio-Tagle & Muñoz-Tuñón 1998; Fielding, Quataert & Martizzi 2017; Schneider, Robertson & Thompson 2018). Studies of the centrally localized outflows provide a foundation of understanding properties of star forming outflows in general case.

The gas ejection speed is a critical parameter necessary for better understanding the processes of gas circulation driven by superwinds and for determining main properties of gas motion that affects the lifecycle of gas in galaxies (Veilleux et al. 2005; Zhang 2018). The speed ranges from hundred (Shopbell & Bland-Hawthorn 1998; Veilleux et al. 2005) to thousand km s^{-1} (Heckman et al. 2000), which leads to the gas loss rate up to 10–20 $M_\odot$ yr^{-1} (Heckman 2002; Chisholm et al. 2015). While galaxies observed at high inclination angles allow us to detect the gas outflows easily (Bizyaev et al. 2019), their geometry does not favour the gas speed measurements. In contrast, objects observed at close to face-on inclination angles would allow us to assess the outflow speed directly.

Large integral field spectroscopic surveys of last years allow us to create large samples of unique galaxies, including the objects with

★ E-mail: dmbiz@apo.nmsu.edu

central, star formation driven outflows. In this paper, we apply the criterion for selecting galaxies with star formation driven biconical outflows derived by Bizyaev et al. (2019) to galaxies with low inclination angles found in the sample of MaNGA survey objects from Bundy et al. (2015). The special orientation of galactic planes makes the visual selection of these objects difficult, but instead it simplifies kinematic studies of such objects. At the same time, elements of galactic structure can be identified with better certainty in the low-inclined galaxies with respect to the galaxies with high inclination studied by Bizyaev et al. (2019), hereafter B19.

2 THE SAMPLE OF STAR FORMATION DRIVEN BICONES FROM MANGA OBSERVATIONS

In this paper, we use a sample of galaxies observed with the Integral Field Unit (IFU) survey MaNGA (Mapping Nearby Galaxies at APO), see Bundy et al. (2015), Drory et al. (2015), Law et al. (2016). The survey was conducted at a 2.5-m telescope (Gunn, Siegmund & Mannery 2006) in the frames of the Sloan Digital Sky Survey (SDSS; York et al. 2000; Blanton et al. 2017; Abdurroúf et al. 2021). MaNGA targeted a large sample of galaxies uniformly distributed in stellar mass (Wake, Bundy & Diamond-Stanic 2017), and achieved a few per cent precision of its flux calibration (Yan et al. 2016b; Yan, Tremonti & Bershady 2016a), two dozen km s^{-1} precision in the emission line velocity dispersion estimation (Law et al. 2021), and a kiloparsec-scale spatial resolution in mapping galaxies at the survey's median redshift of 0.03 (Yan et al. 2016b). MaNGA has released its complete sample of 10 050 galaxies in the frames of the data release SDSS DR17 (Abdurroúf et al. 2021). The released data products include maps of emission line fluxes and radial velocities in gas and stellar population (Westfall et al.) which continuously cover most parts of the galaxies.

We select low inclination galaxies from the whole MaNGA sample based on photometric estimates of the inclination angles from the parent catalogue NSA (NASA-Sloan Atlas; Blanton, Kazin & Muna 2011). For the galaxies with the inclination angle below 45 degrees, we apply a criterion for selecting galaxies with star formation driven bicones using the 'figure of merit' F derived by Bizyaev et al. (2019) as follows:

$$F = \log\left[\Sigma_{\rm SFR}^{1/2} Z_c/\sigma_c\right] - 2\log R_e, \quad (1)$$

where the star formation rate surface density $\Sigma_{\rm SFR}$ is measured at the centre from the Hα luminosity, $Z_c = \tau_V 40 * 10^{(O/H)}$ at the centre, τ_V is the optical depth proportional to the extinction A_V estimated from the Balmer decrement via fluxes in emission lines, $\sigma_c = 1.65(0.33 v_c - 2)$, v_c is the maximum rotation velocity and R_e is the effective radius of the galaxies. We select the galaxies with F > -5.0. Additionally, we require that the central gas velocity dispersion exceeds the stellar velocity dispersion. We select 326 galaxies with low inclination and high values of the figure of merit. As it follows from Bizyaev et al. (2019), the 'figure of merit' is based on a combination of metallicity, extinction, star formation rate density, central velocity dispersion, and the compactness of the central galactic region. The F is a single parameter that allows us to distinguish between the galaxies with star formation driven biconical outflows and regular galaxies. Fig. 9 in Bizyaev et al. (2019) shows that the former galaxies prefer to have high F values, which indicates high star formation surface density, high metallicity and large compactness at their central regions. Objects with F > -5.0 have a high probability to harbour the star formation driven bicones. Significantly lower values of the F allow us to select regular galaxies for comparison purposes, see below.

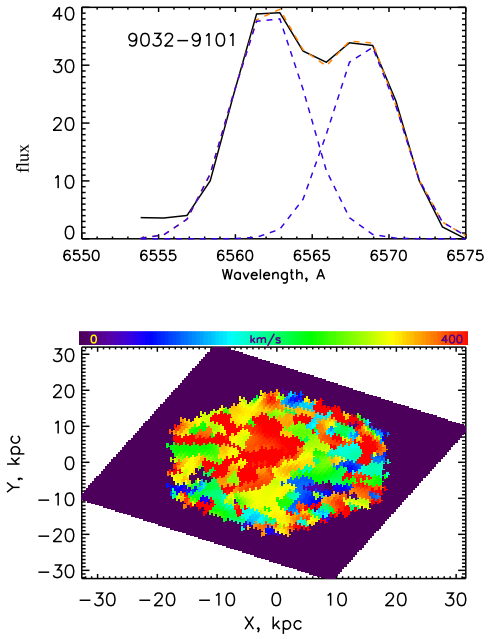

Figure 1. Top: An example of double picked line profile for one of our galaxies with biconical outflow and our Gaussian fitting. The solid black line designates the observing line profile, the blue dashed lines show two Gaussians separately, while the red dashed line demonstrates the sum model profile. Bottom: the distribution of the gas velocity dispersion in a FSFB galaxy.

After browsing SDSS images (Abdurroúf et al. 2021) of the candidates we removed the cases of galaxy mergers, which includes all cases of objects with overlapping bodies significantly distorted by interactions. The BPT diagrams (Baldwin, Phillips & Terlevich 1981) of remained objects were inspected and only the galaxies with star forming centres were left in the sample. Only the central 3x3 spaxel areas were considered.

As the next step, we analysed Hα emission line profiles in the central spaxel and found that most of selected face-on galaxies with central star formation driven biconical gas outflows (FSFB) have widened lines or show clear double peak profiles. We fit the line profiles with double Gaussians. We assume that the blue Gaussian line is associated with approaching side of gas outflow, while the red Gaussian component corresponds to its receding side. We find that the central line profiles of 116 galaxies out of 248 can be successfully fitted with a single Gaussuan, while 132 galaxies (53 per cent) require two Gaussians. An example of a Gaussian fitting is shown in Fig. 1 in the top panel. The bottom panel shows that the gas velocity dispersion is also high at the centres of the galaxies with wide central emission lines.

To ensure that the FSFB sample has wider emission lines with respect to the control sample, we aim to compare the central Hα emission line profile among the two sample and to compare a prominent absorption line profile at the same time. Fig. 2 compares averaged profiles of Hα emission line (top panel) and averaged profiles of a prominent absorption Mgb line (bottom) for both samples of galaxies - FSFB and control. The line profiles are considered at the central spaxel of the galaxies. Note that all line profiles in Figs 1 and 2 are corrected to the radial velocity that corresponds to zero stellar velocity, which corresponds to the wavelength of Hα line in vacuum (6564.6 Å). The selected FSFB galaxies have systematically wider emission line profiles, while the absorption line profile does not show

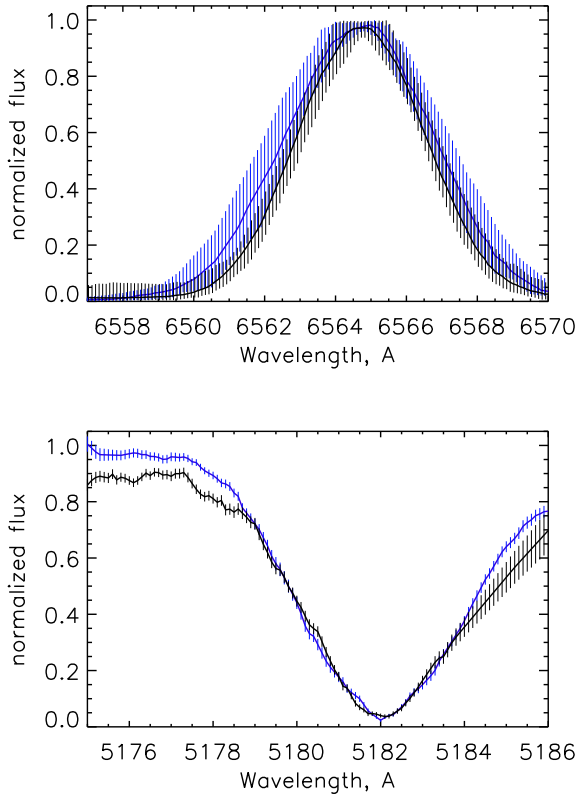

Figure 2. Top: the median co-added profiles (solid curves) of the Hα line for the FSFB (blue) and comparison (black) galaxies. The error bars show 10 and 90 percentile curves for both samples. Bottom: the same for the Mgb absorption feature. It is seen that the FSFB sample has wider average Hα line profile, while the Mgb absorption feature has the same width for both samples of galaxies.

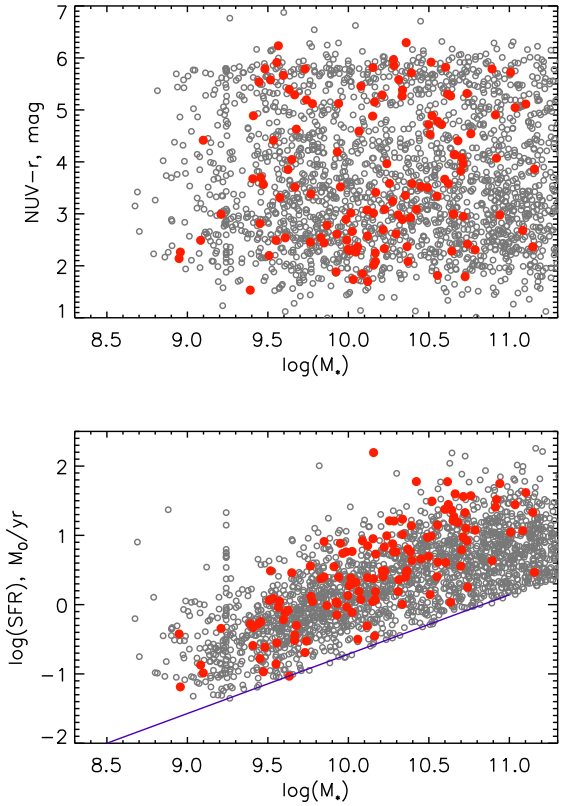

Figure 3. The MaNGA galaxies with biconical outflows (FSFB, red bullets) and without them (grey circles, comparison sample) are shown on the SFR - Stellar Mass diagrams. Top: the near-ultraviolet - red magnitude difference from the NSA, as a proxy for the specific star formation rate. Bottom: the stellar mass is taken from the NSA catalogue, while the integrated star formation rate is estimated via the Hα fluxes provided by MaNGA. The solid line demarcates star forming objects (above) from green valley and quiescent galaxies (Chang et al. 2015).

significant difference between the samples. Note that the combined Hα line profile for the FSFB sample is a combination of double-peaked and widened profiles, so although the combined curve doesn't indicate distinctive double-peaked shape, it has a wide, flat top, and large error bars. Being more narrow, the combined profile for the comparison objects is closer to a single Gaussian shape. It can be seen that the emission line profiles are symmetric with respect to the zero velocity of the stellar component. This suggests that we observe the biconical outflows rather than the blue outflow peak and the redder peak corresponding to the centre of the galaxy.

As a result, we selected 132 galaxies, which we refer to as 'face-on galaxies with star formation driven biconical outflows' or FSFBs. We also inspected velocity fields of emission gas and stars in all of these galaxies and found 16 cases of significant misalignment between stellar and gas kinematics, with position angles difference exceeding 30°, according to the KINEMETRY package (Krajnović et al. 2006).

We aim to compare the FSFB objects with 'regular galaxies', so we make a comparison sample of galaxies with similar properties but without the biconical outflows. We started with selecting low inclination galaxies the same way as described above, then we reverted the selection criterion and left only objects with $F < -5.3$. We checked the central Hα line profiles the same way as for the FSFB group and found only 8 out of 483 objects with widened Hα profiles at their centres, which require two Gaussians to fit the Hα line profile. These galaxies were removed from the comparison group. Note that all these 8 galaxies are found in objects with noticeable interaction with their satellites. We inspected optical SDSS images of the comparison galaxies and removed 60 more cases of merging galaxies.

When we place the FSFB and comparison groups on the star formation rates (SFR) versus stellar mass (M_*) diagrams in Fig. 3, we notice that all FSFB galaxies are located above the line that demarcates star forming and green valley galaxies, according to Chang et al. (2015). While most of the objects in the comparison sample are located above this demarcation line, too, a small fraction of them lays in the 'green valley' region. We removed those objects from the comparison sample. As a result, the comparison group comprises 375 galaxies. The resulting distribution on the SFR-M_* diagram is demonstrated in Fig. 3.

As a consistency check, we plot histogram distributions of radial velocities for the selected groups of galaxies, see Fig. 4. The histograms ensure that galaxies in our FSFB and comparison samples have rather similar distance distributions.

3 PROPERTIES OF THE GALAXIES WITH STAR FORMATION DRIVEN BICONES

3.1 Structural parameters

Our selection procedure with equation (1) intentionally biases the parameters of FSFB galaxies with respect to the control sample, so we expectantly see systematic differences in the effective radius and

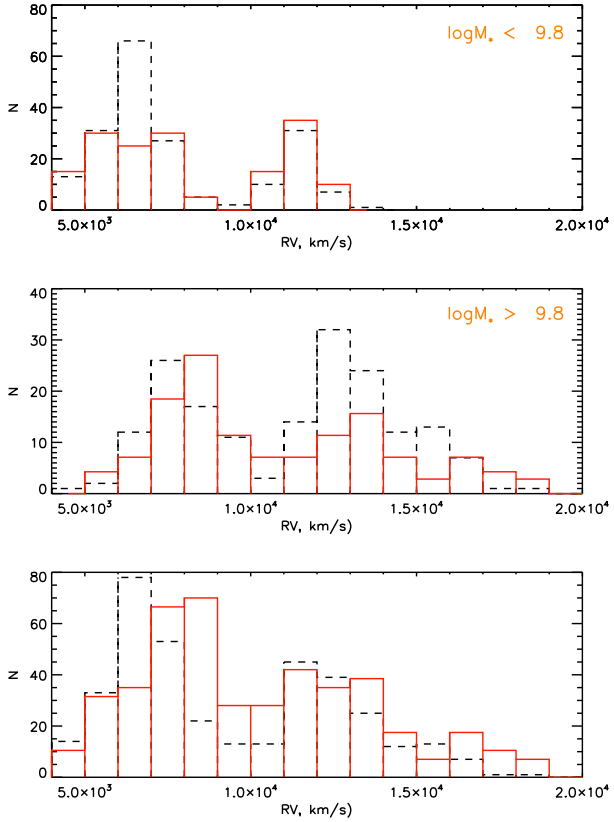

Figure 4. Radial velocities of selected face-on galaxies with SFB (red line) and comparison galaxies (black dashed line). The top and middle panels show low- and high-mass galaxies, respectively. The bottom panels shows all mass groups together.

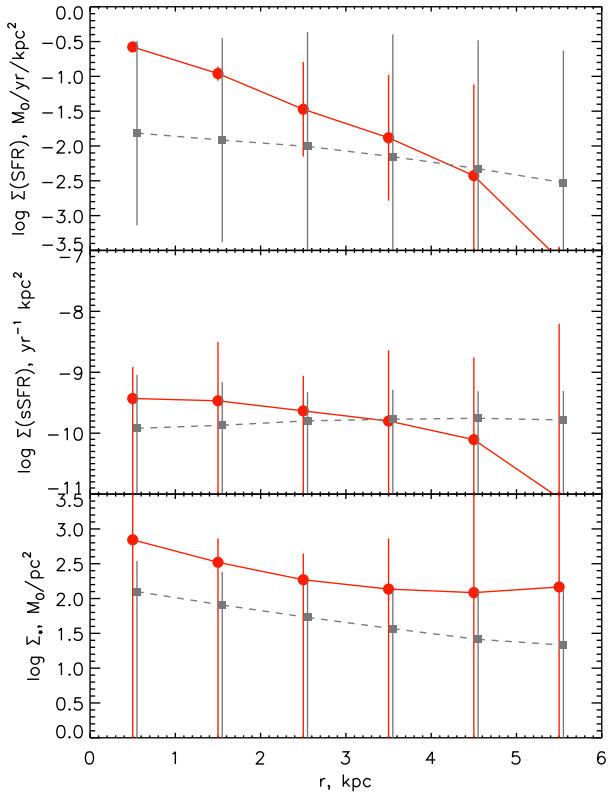

Figure 5. The median values and 1-σ error bars for the star formation rate surface density (top), specific star formation rate surface density (middle), and stellar surface density (bottom) for the FSFB galaxies (red symbols and solid lines) and control sample (grey symbols and dashed lines).

metallicity between the two samples. Given the face-on orientation of galaxies in our samples, we can study the radial distributions of parameters without significant projection effects, which makes our comparison between the samples more straightforward than that for the galaxies with high inclination used by Bizyaev et al. (2019).

Fig. 5 shows how the surface density of star formation, specific star formation (defined as sSFR = SFR/M_* or as the similar ratio of the surface densities), and stellar mass densities change with radius. We stacked values in annuli regularly spaced along the radius. The bullets and error bars correspond to the mean and standard deviation values, respectively. Similar to B19, we see a significantly enhanced central concentration of star formation rate in the FSFB galaxies - only in the very central radial bins. The specific star formation rate is not significantly different between the main and control samples. We highlight this difference even more in Fig. 6, where the Hα concentration is shown for low- ($\log M_*/M_\odot < 9.8$) and high-mass ($\log M_* < 9.8/M_\odot$) galaxies. Same as in B19, the Hα concentration is estimated as the ratio of Hα luminosity within and outside the central 1 kpc circle. While the fraction of centrally concentration is higher in massive FSFB galaxies with respect to the comparison objects, this difference becomes especially prominent in the low mass galaxies.

3.2 Stellar population

While properties of stellar population in the galaxies observed at high inclination angles studied by B19 is affected by projection effects, face-on orientation allows to consider a more clear case. Fig. 7 shows results of a linear fitting of D(4000) radial index distribution in each galaxy: the index central value and its radial gradient. Low mass FSFB galaxies have more objects with positive D(4000) gradients than the comparison galaxies. The central values have more scatter in them, and the distribution reveals more FSFB objects with high central values of the index. High mass FSFB sample have even a higher fraction of galaxies with positive radial gradient of D(4000), while their central values are the same as in the comparison galaxies.

According to numerical estimates of the D(4000) index by Kauffmann et al. (2003a), the main age of stellar population in our massive galaxies is of the order of 1 Gyr in both samples. Centres of low massive comparison galaxies are younger, while the FSFB galaxies from this mass range are often a few times older. Both low mass and especially high mass FSFB galaxies often have significant positive radial gradient of stellar population age.

Fig. 8 shows the mean value of D(4000) index and its error of the mean determined in 1 kpc wide radial annuli evenly distributed along the radius. While the centres of the galaxies have essentially the same age between the samples, FSFBs show consistently higher positive gradient with respect to the comparison sample. FSFB objects have younger stellar population at their centres in the comparison with the rest of the galaxy. The regular galaxies, in contrary, have older centres with respect to their periphery.

The radial gradient of the [α/Fe] index demonstrated in Fig. 9 does not show significant difference between the FSFB and control samples. Although the histogram distributions look slightly different for the low- and high-mass galaxies in the left-hand panels, the mean and mode values of the distributions for the FSFB and control galaxies look similar. In contrast, FSFB galaxies of all masses often show higher [α/Fe] at their centres than at the periphery. This can be

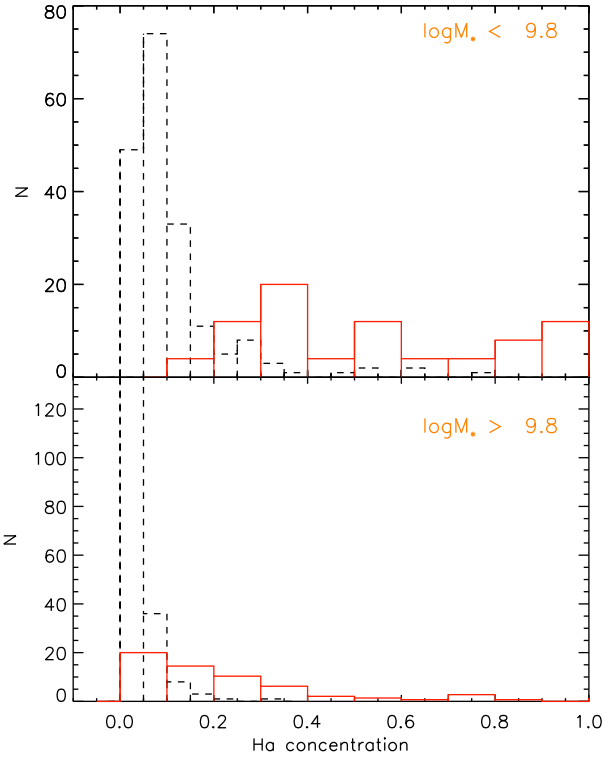

Figure 6. Concentration of Hα emission in low- (upper panel) and high-mass (lower panel) galaxies. The designation is kept the same as in Fig. 4.

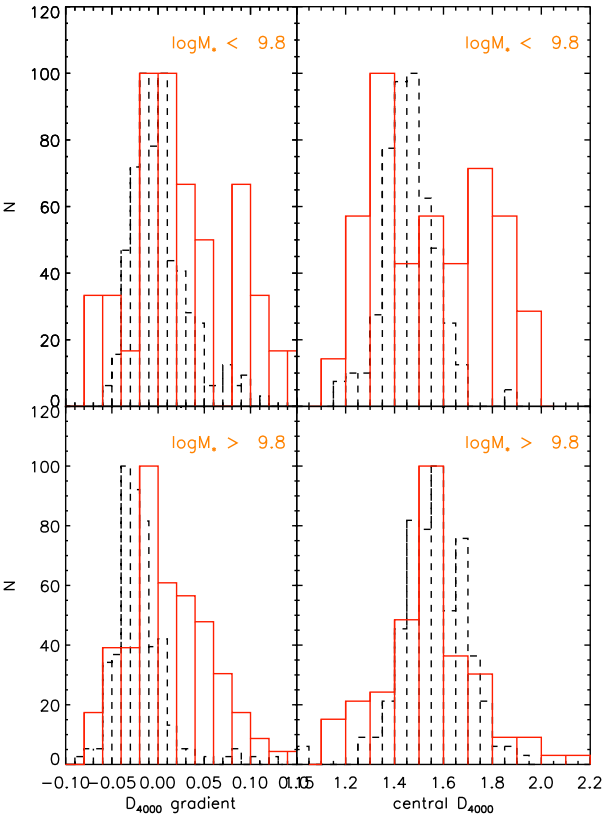

Figure 7. The central values and radial gradient of D(4000) index for the FSFB (solid red lines) and control galaxies (dashed black lines) for low- and high- mass galaxies (top and bottom panels, respectively).

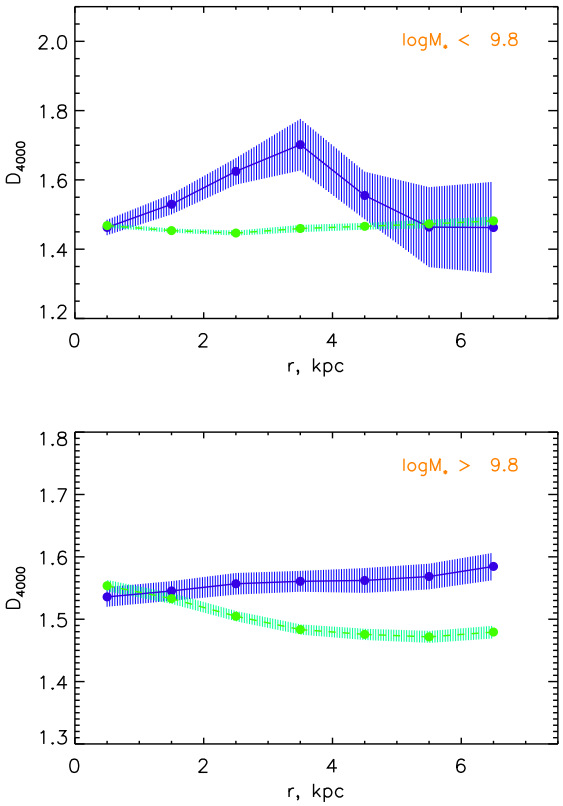

Figure 8. Cumulative radial distributions of mean D(4000) index (curves) and its errors of mean (shaded areas) for FSFB (blue) and comparison (green) galaxies. The panels correspond to the low- (top) and high-mass (bottom) galaxies.

interpreted as a significant contribution of the recent starburst (within the last Gyr) to the formation of galactic centres of FSFB objects.

3.3 Kinematics of ionized gas

While the face-on orientation of galactic midplanes makes difficult their selection, it simplifies measuring the outflow velocities. As it was mentioned in §2, we analyse Hα emission line profiles at the central spaxel. All galaxies in our sample have wide or double profiles that need to be fitted with two Gaussian lines. Many galaxies have clearly separated double peaks. Velocities of the blue (v_{blue}) and red (v_{red}) peaks of fitted Gaussians are assigned to the approaching and receding sides of ionized gas outflows. We assume that the mean central outflow speed is equal to $V_{out} = 0.5(v_{red} - v_{blue})$. We also assume that the full width at half-maximum (FWHM) of the Gaussians dV_{out} indicates the real velocity distribution in the outflows, and that the maximum gas ejection speed is $V_{max} = \sqrt{V_{out}^2 + dV_{out}^2}$.

Fig. 10 shows the histogram distributions of the V_{out}, dV_{out}, and V_{max} in our FSFB galaxies. Out of all galaxies FSFB, 16 objects have counter-rotating gas and stellar discs. We mark these galaxies with the red-dashed line in Fig. 10. It is seen that the subsample of counter-rotators has the same histogram distributions as the main FSFB sample. The mean and median values of the outflowing gas speed are shown in Table (1). Note that our maximum speed is consistent with the gas outflow speed if it were measured via the maximum profile width.

Heckman (2002) found that the star formation outflows occur when the star formation surface density exceeds certain limit, e.g.

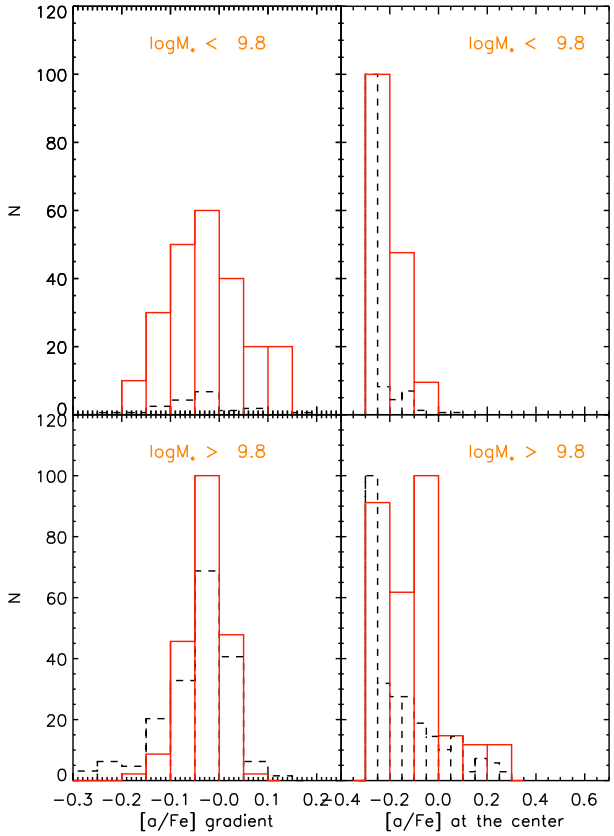

Figure 9. The central values and radial gradient of [α/Fe] index for the FSFB (solid red lines) and control galaxies (dashed black lines) for low- and high-mass galaxies (top and bottom panels, respectively).

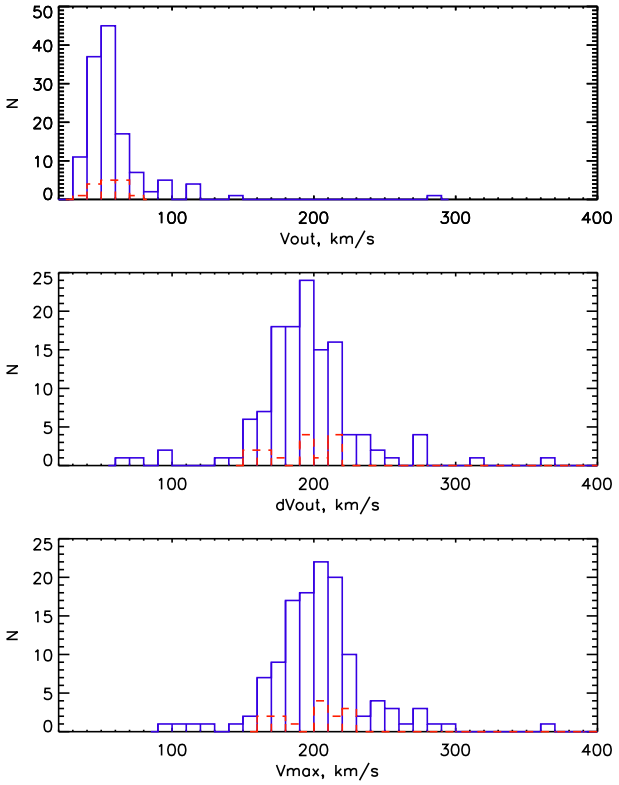

Figure 10. Histogram distributions of gas outflow kinematic characteristics for the FSFB galaxies. Top: the peak outflow speed in km s^{-1}. Middle: the FWHM of the outflow component in FSFB in km s^{-1}. Bottom: maximum outflow speed in km s^{-1}, see text. The blue line designates all FSFB galaxies, while the red dashed line highlights the galaxies with counter-rotation between their gas and stars.

0.1 $M_\odot$ yr^{-1} kpc^{-2}. Fig. 11 shows that we have significant number of galaxies in our sample whose central star formation rate surface density is in the range from 0.01 to 0.1 $M_\odot$ yr^{-1} kpc^{-2}. Fig. 11 demonstrates how the peak outflow speed, its FWHM, and maximum outflow speed depend on the star formation surface density at the centres of FSFB galaxies.

Fig. 11 shows that the peak gas velocity does not depend significantly on the central star formation activity SFR_c, while the gas velocity dispersion in ejected ionized gas is mildly correlated with the SFR_c. A linear regression fit to the latter relation has a slope of 0.18. This case better corresponds to the case of the gas velocity dispersion caused by the Jeans instability in clumps, according to Elmegreen et al. (2007), Lehnert et al. (2009). In this case $\sigma_{gas} \sim \Sigma_{SFR}^{0.18}$, which is designated with the solid red line in the middle panel. The small slope of the observing FWHM - Σ_{SFR} relation is also in agreement with the turbulence dissipation model by Dib, Bell & Burkert (2006), Lehnert et al. (2009), where $\sigma_{gas} \sim \Sigma_{SFR}^{1/3}$ (shown with the solid-blue line). The green line designates the case of turbulence driven by gravitational instabilities Lehnert et al. (2009), Krumholz & Burkhart (2016), which implies $\sigma_{gas} \sim \Sigma_{SFR}^{0.5}$. This slope is too steep for our sample, see the green-dashed line in the middle panel.

It is hard to measure the volume density of the ejected gas directly because of projection effects. At the same time, we can easily measure the size of the Hα-emitting nucleus and guess its gas content. The size can be estimated directly as the radius where the Hα emission surface density drops e times from its central value. While we cannot measure the gas surface density directly, we can use the Kennicutt–Schmidt relation between the gas surface density and the star formation rate from Kennicutt (1998) which, in turn, is a function of the Hα luminosity density (Martin & Kennicutt 2001). In the assumption of spherical geometry of the region with the starburst and biconical outflow, we estimate the gas mass M_g, its volume density and the mass outflow rate $(dM/dt)_{out}$. Fig. 12 shows the gas outflow exhaust time t_e in the upper panel, which is defined from the central gas mass and the gas outflow rate as $t_e = M_g/(dM/dt)_{out}$. There is no clear trend of $(dM/dt)_{out}$ and t_e with the galactic mass. The median value of t_e is 46 Myr. The bottom panel in Fig. 12 demonstrates the ratio of the gas outflow rate to the star formation rate. The ratio is less than one in all galaxies, which is consistent with similar estimates for other types of galaxies (e.g. Concas, Maiolino & Curti 2022). This ratio is systematically low in massive galaxies, while in low mass objects it reaches 50 per cent.

Table 1. The mean and median peak outflow speed, FWHM, and maximum outflow speed for the sample of FSFB galaxies.

	Mean km s^{-1}	Median km s^{-1}
V_{out}	58	53
dV_{out}	203	195
V_{max}	212	205

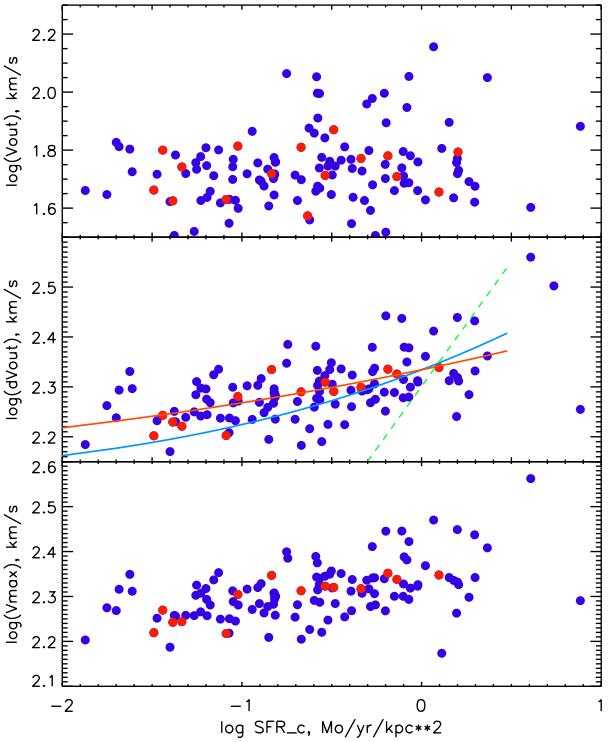

Figure 11. The peak outflow speed (top), its FWHM (middle) and maximum outflow speed (bottom) versus the star formation surface density at the centres of FSFB galaxies. The blue symbols designate all FSFB galaxies, while the red ones mark the galaxies with counter-rotation between their gas and stars. The red, blue, and green curves in the middle panel correspond to the gas velocity dispersion caused by the Jeans instability in clumps, the turbulence dissipation, and the turbulence driven by gravitational instabilities, respectively (see text).

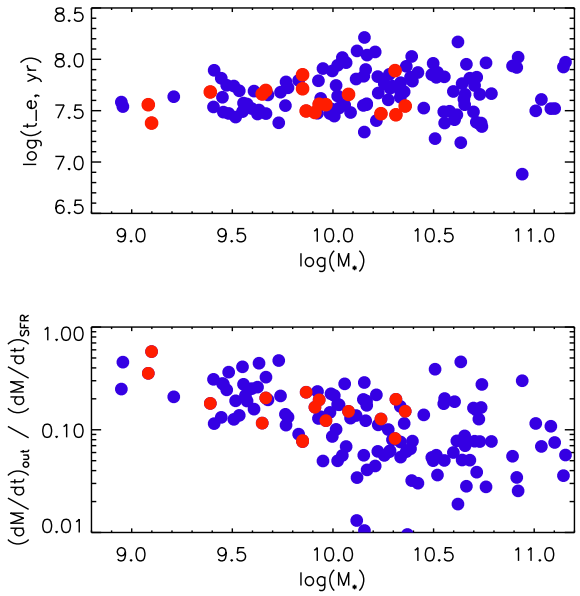

Figure 12. Top: the central gas exhaust time for FSFB galaxies of different stellar mass. Bottom: the ratio of the mass outflow rate to the star formation rate at the centre of FSFB versus the galactic stellar mass. The blue symbols mark all FSFB galaxies, while the red ones highlight the galaxies with counter-rotation between their gas and stars.

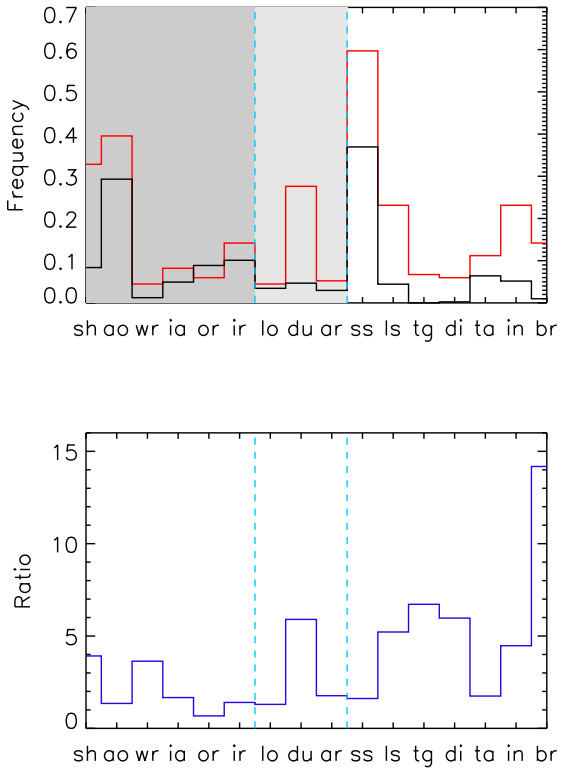

Figure 13. Upper panel: the lines show the frequency of environmental features (shown on the *x*-axis) among the entire sample of FSFB (red) and comparison (black) objects. The areas are shaded differently according to the age of the features (old-intermediate-young from the left to the right, see text). Lower panel: The ratio of FSFB to the control galaxies in each bin from the upper panel. The vertical blue-dashed lines demarcate the features of different age, same as in the upper panel.

3.4 Environment of the galaxies

Here we study the difference in environment between the two samples. Two types of environmental features are considered. First, we visually inspect images of the galactic vicinity at distances comparable to their size using optical SDSS[1] and DES Legacy[2] images.

Atkinson, Abraham & Ferguson (2013) identified a variety of low surface brightness structures that can be found around regular galaxies. Adopting technique from Atkinson et al. (2013), we identify a set of structural elements for each galaxy in both FSFB and comparison samples. The elements include nearby small satellites (ss), nearby large satellites (ls), low surface brightness loops (lo), shells (sh), arcs (ar) around the galaxies, tails (ta), bridges (br), noticeable asymmetry of outer isophotes (ao), irregular dust lanes crossing bodies of galaxies (du), inner (ir) and outer (or) rings, significant inner asymmetry (ia), and wrecked shape (wr). We also notice the shape disturbance caused by interaction (di), membership of a tight group (tg), and an interaction with a companion (in). We distinguish the latter from merging, when two or more objects are forming single stellar structure.

In addition to looking for structural peculiarities in and around the galaxies, we widen the field of consideration and count the number of small or large satellites in 15 arcmin fields centred at the galaxies.

[1] http://skyserver.sdss.org
[2] http://legacysurvey.org/pubs/

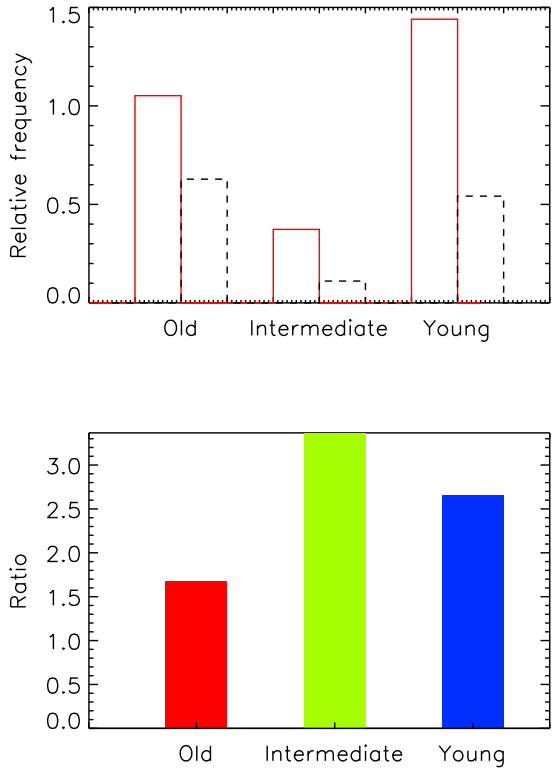

Figure 14. Top: The relative frequency of features from Fig. 13 combined by their age of the interaction for the FSFB (red-solid line) and comparison (black-dashed line) samples. Bottom: the ratio of the frequencies from the top panel.

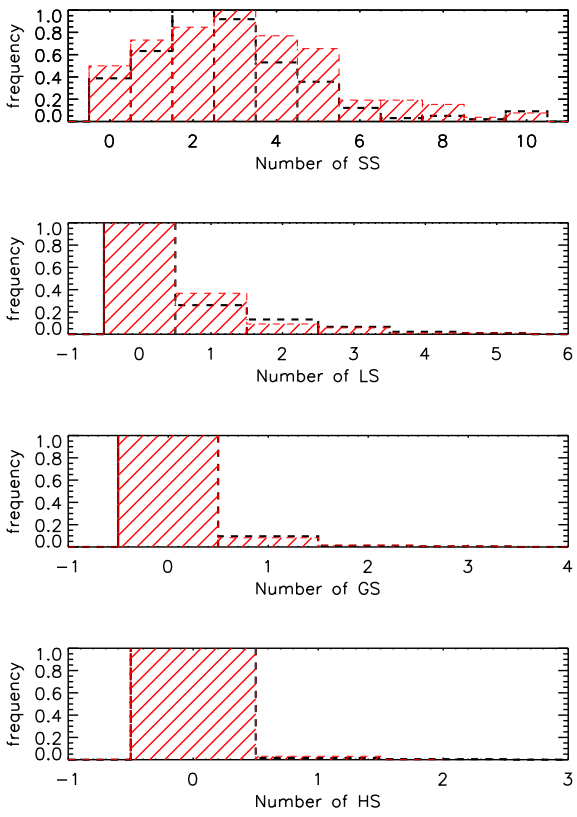

Figure 15. Histogram distributions of the number frequency of satellites around the FSFB (red lines) and comparison (black dashed lines) galaxies separated by their size (small to large, from top to bottom).

We record the number of the following elements: small satellite (SS - very small galaxies around, not taken into account in the narrow fields considered above); large satellite (LS - large enough galaxies with recognized internal structure, but still less in size than the main galaxy); even larger satellite (GS - comparable to the main galaxy or slightly larger); and huge satellite (HS - much larger companion in the field). Note that some of the SS and HS can result from the objects projection and not from the real proximity in space.

The upper panel in Fig. 13 demonstrates the frequency of the structure elements defined above in the FSFB (red line) and control (black line) samples. The lower panel in Fig. 13 shows the same information as a division of the FSFB frequency by that of the comparison sample, determined for each environmental element. Note that some structural elements are rarely found in the comparison galaxies, so the results of the division shown in the lower panel are not reliable numerically, albeit significant. We notice significantly enhanced fraction of nearby large satellites, shells, peculiar dust lanes, disturbed or wrecked shape, signs of interaction, including bridges, and association with tight groups in the FSFB objects with respect to the comparison galaxies.

We subdivide the environmental features around the galaxies by three classes based on their interaction stage: young (ss, ls, tg, di, ta, in, br), intermediate (lo, du, ar) and old (sh, ao, wr, ia, ir, or). When combined by their age of interaction, the structural elements also demonstrate difference between the samples of galaxies. Fig. 14 shows a relative frequency of the elements in the upper panel for the FSFB (red) and control sample (black). Their ratio is shown in the lower panel, which reveals the most significant difference between the samples of objects with the young and intermediate age features.

Fig. 15 demonstrates the frequency of satellites between the two groups of galaxies. While the large neighbours, like GS, HS, and also LS, show no difference between the samples, the number of smallest satellites is enhanced around the FSFB objects.

4 DISCUSSION

Studying MaNGA galaxies observed at low inclination angle allows us to verify and complete conclusions made in the previous work by B19. Employing advantages of low inclination, we can measure the gas outflow speed directly. The surface density of the star formation rate also can be studied without any projection effects. Figs 5 and 6 confirm that the face-on galaxies with star formation driven bicones have high central concentration of Hα emission and star formation, especially in galaxies with low mass. Radial distributions of the stellar population age look special for the FSFB galaxies. Figs 7, 8, and 9 suggest that while galaxies in the comparison sample have older centres and younger peripheries, the FSFB objects in contrary have younger central regions. The D(4000) and [α/Fe] distribution in them suggest that the bulk stellar population at the centres was formed within last Gyr.

Fig. 11 demonstrates that although most of the bicones have their central star formation rate surface density above 0.1 $M_{\odot}/pc^2$, a noticeable fraction of them indicates lower star formation rate density between 0.01 and 0.1 $M_{\odot}/pc^2$.

Our FSFB galaxies have moderate peak outflow velocity estimated directly either from a double peaked profile or from broadened emission line at the centre, see Fig. 10. Fig. 11 compares the velocity and its dispersion in gas with central star formation surface density, and helps make conclusion that the Jeans instability in star formation clumps and also the turbulence dissipation in gas drive the gas turbulence in the central regions of galaxies with biconical gas outflows and provide a small slope of the $\sigma_c \div \Sigma_{SFR}$ relation there.

Our estimate of the gas outflow rate and of the central gas exhaust time shows no difference between low- and high-mass galaxies. The exhaust time-scale is rather short, 46 Myr on average. The gas outflow plays a more significant role in the gas depletion process in low mass FSFB galaxies with respect to the star formation. In contrast, star formation is the dominating process that regulates the gas consumption at the centres of massive galaxies, where the gas outflow contributes only a small fraction to the gas depletion process. At the same time, centres of all our FSFB galaxies convert more gas to the stars than eject to the circumgalactic medium.

Comparison between the FSFB and control samples of galaxies allows us to conclude that some features coincide with the central star formation driven biconical outflows. Thus, the frequency of shells, inner rings, and unusual dust pattern is much higher in the FSFB objects, as well as such signs of ongoing or recent interaction as disturbed or wrecked shape, bridges between galaxies or presence of nearby large neighbours, as well as membership in tight galactic groups. The presence of four or more small satellites is also a feature more often seen around the FSFB objects.

All features of FSFB galaxies mentioned above suggest that the galaxies experience starbursts at their centres that enhance the fraction of young stellar population. The small- and large-scale gas turbulence caused by the starburst helps eject metal enriched gas with the peak speed of the order of 60 km s^{-1} , and maximum speed over 200 km s^{-1} . At the same time, the star formation consumes much more gas than massive galaxies eject, while low mass galaxies lose their gas via its outflow more intensively with respect to its depletion by star formation. Interaction with nearby satellites, ongoing and past, as well as some low surface brightness environmental structures reveal evidences of connection between the central gas outflow and interaction with environment in the FSFB galaxies. In a combination with younger centres in the FSFB galaxies, we can assume that minor interactions are responsible for driving gas to the centres of galaxies, where it fuels intensive starbursts.

Given the much shorter time-scale of the gas exhausting at the centre (dozens of Myr) in the comparison with the age of central stellar population (a few hundred Myrs), we can conclude that the gas at the centre needs to be replenished. Minor interactions with gas-rich satellites should be a source of fresh gas. Gas supply from the circumgalactic medium should also play some role, but we don't clearly see sources of this kind of accretion in our data.

We notice that FSFB galaxies with significant misalignment between gas and stars show the same features, trends, and numerical estimates as the galaxies with regular gas and stellar rotation. Since the counter-rotation is a direct evidence of past interactions of galaxies with their satellites, we are enabled to conclude that such interaction might take place in the past of all other FSFB galaxies.

5 SUMMARY

We select 132 galaxies with low inclination and with biconical gas outflow from the centres driven by star formation processes (FSFB) from the final MaNGA data release. Our selection procedure is based on a combination of general galactic parameters that can be determined from photometry and spectroscopy, not necessarily panoramic. It means that the selection procedure can be run for a much wider samples available from the modern sky surveys. We form a sample of comparison sample of 375 galaxies with similar characteristics. All FSFB galaxies show either double peaked or broadened emission lines at their centres. We estimate that the mean peak outflow gas velocity is 58 km s^{-1}, and the mean maximum gas velocity is 212 km s^{-1}. The slope of the gas velocity dispersion versus the star formation rate surface density at the centre is small, which suggests that the gas dispersion is powered by the Jeans instability in gas clumps or by the gas turbulence dissipation.

We conclude that the gas loss rate is significant at the centres of small galaxies with respect to the gas depletion via star formation processes, while in large galaxies the latter is the principal process of the central gas depletion. In combination with a median gas depletion scale of 46 Myr typical for galaxies of all masses and the mean stellar population age of a few hundred Myrs, we conclude that the central gas should be refilled, most probably from the accretion of small satellites. The latter is confirmed by enhanced frequency of young and intermediate age features and high number of small satellites that we see around the FSFB objects, with respect to the comparison galaxies.

Our FSFB sample has 16 galaxies with significant misalignment between kinematics of their gas and stars. These galaxies show the same trends, features, and numerical values as all other FSFB objects with regular rotation, which also suggests that past interactions with small satellites played significant role in supplying gas to the central regions of galaxies and in the consequent formation of star forming driven biconical gas outflows.

ACKNOWLEDGEMENTS

The authors would like to thank the anonymous referee for constructive comments that improved the paper. YC acknowledges support from the National Key R&D Program of China (No. 2017YFA0402700), the National Natural Science Foundation of China (NSFC grants 11573013, 11733002) YS acknowledges support from the National Key R&D Program of China (No. 2018YFA0404502) and the National Natural Science Foundation of China (NSFC grants 11733002 and 11773013). The project is partly supported by RSCF grant 22-12-00080. RR thanks to Conselho Nacional de Desenvolvimento Científico e Tecnológico (CNPq, Proj. 311223/2020-6, 304927/2017-1, and 400352/2016-8), Fundação de amparo à pesquisa do Rio Grande do Sul (FAPERGS, Proj. 16/2551-0000251-7 and 19/1750-2), Coordenação de Aperfeiçoamento de Pessoal de Nível Superior (CAPES, Proj. 0001). RAR acknowledges financial support from Conselho Nacional de Desenvolvimento Científico e Tecnológico (CNPq – 302280/2019-7) and Fundação de Amparo à pesquisa do Estado do Rio Grande do Sul (FAPERGS – 21/2551-0002018-0). JGF-T gratefully acknowledges the grant support provided by Proyecto Fondecyt Iniciación No. 11220340, and also from ANID Concurso de Fomento a la Vinculación Internacional para Instituciones de Investigación Regionales (Modalidad corta duración) Proyecto No. FOVI210020, and from the Joint Committee ESO-Government of Chile 2021 (ORP 023/2021).

SDSS-IV acknowledges support and resources from the Center for High-Performance Computing at the University of Utah. The SDSS web site is www.sdss.org.

SDSS-IV is managed by the Astrophysical Research Consortium for the Participating Institutions of the SDSS Collaboration including the Brazilian Participation Group, the Carnegie Institution for Science, Carnegie Mellon University, the Chilean Participation Group, the French Participation Group, Harvard-Smithsonian Center for Astrophysics, Instituto de Astrofísica de Canarias, The Johns Hopkins University, Kavli Institute for the Physics and Mathematics of the Universe (IPMU) / University of Tokyo, Lawrence Berkeley National Laboratory, Leibniz Institut für Astrophysik Potsdam (AIP), Max-Planck-Institut für Astronomie (MPIA Heidelberg), Max-Planck-Institut für Astrophysik (MPA Garching), Max-Planck-Institut für Extraterrestrische Physik (MPE), National Astronomical

Observatory of China, New Mexico State University, New York University, University of Notre Dame, Observatrio Nacional / MCTI, The Ohio State University, Pennsylvania State University, Shanghai Astronomical Observatory, United Kingdom Participation Group, Universidad Nacional Autónoma de México, University of Arizona, University of Colorado Boulder, University of Oxford, University of Portsmouth, University of Utah, University of Virginia, University of Washington, University of Wisconsin, Vanderbilt University, and Yale University.

DATA AVAILABILITY

This work makes use of SDSS/MaNGA project data publicly available at https://www.sdss.org/dr17/data_access/.

REFERENCES

Abdurroúf et al., 2021, ApJS, 259, 39
Atkinson A. M., Abraham R. G., Ferguson A. M. N., 2013, AJ, 765, 28
Baldwin J. A., Phillips M. M., Terlevich R., 1981, PASP, 93, 5
Bizyaev D. et al., 2019, ApJ, 882, 145 (B19)
Blanton M. R. et al., 2011, AJ, 142, 31
Blanton M. R. et al., 2017, AJ, 154, 28
Bundy K. et al., 2015, ApJ, 798, 7
Chang Y.-Y., van der Wel A., da Cunha E., Rix H.-W., 2015, ApJS, 219, 8
Chen Y.-M. et al., 2010, AJ, 140, 445
Chisholm J. et al., 2015, ApJ, 811, 149
Concas A. et al., 2022, MNRAS, 513, 2535
Davies R. et al., 2018, ApJ, 873, 22
Dib S., Bell E., Burkert A., 2006, ApJ, 638, 797
Drory N. et al., 2015, AJ, 149, 77
Elmegreen D. M., Elmegreen B. G., Ravindranath S., Coe D. A., 2007, ApJ, 658, 763
Fielding D. et al., 2017, MNRAS, 470, 39
Gunn J. E., et al., 2006, AJ, 131, 2332
Heckman T., 2002, ASP Conf. Proc. 2002., 254, 292
Heckman T., Armus L., Miley G., 1990, ApJS, 74, 833
Heckman T., Lehnert M., Strickland D., Armus L., 2000, ApJS, 129, 493
Heckman T., et al., 2015, ApJ, 809, 147
Kauffmann G., Heckman T., White S., Charlot S., 2001, MNRAS, 341, 54
Kennicutt R., 1998, ARA&A, 36, 189
Krajnović D., Cappellari M., de Zeeuw P. T., Copin Y., 2006, MNRAS, 366, 787
Krumholz M. R., Burkhart B., 2016, MNRAS, 458, 1671
Law D. R. et al., 2016, AJ, 152, 83
Law D. R. et al., 2021, AJ, 161, 52
Lehnert M D., Heckman T. M., Weaver K. A., 1999, ApJ, 523, 575
Lehnert M., Heckman T., 1995, ApJS, 99, 173
Lehnert M., Heckman T., 1996, ApJ, 462, 651
Lehnert M. D. et al., 2009, ApJ, 699, 1660
Martin C. L., Kennicutt R. C., Jr, 2001, ApJ, 555, 301
Rubin K., et al., 2014, ApJ, 794, 156
Schneider E. E., Robertson B. E., Thompson T. A., 2018, ApJ, 862, 56
Shopbell P. L., Bland-Hawthorn J., 1998, ApJ, 493, 129
Strickland D., Heckman T., 2007, ApJ, 658, 258
Tenorio-Tagle G., Muñoz-Tuñón C., 1998, MNRAS, 293, 299
Veilleux S., Cecil G., Bland-Hawthorn J., 2005, ARA&A, 43, 769
Wake D. A., et al., 2017, AJ, 154, 86
Yan R., et al., 2016a, AJ, 151, 8
Yan R., et al., 2016b, AJ, 152, 197
York D. et al., 2000, AJ, 120, 1579
Zhang D., 2018, Galaxies, 6, 114

This paper has been typeset from a TEX/LATEX file prepared by the author.